

# PAS kinase is required for normal cellular energy balance

Huai-Xiang Hao\*, Caleb M. Cardon\*, Wojtek Swiatek\*, Robert C. Cooksey†, Tammy L. Smith\*, James Wilde\*, Sihem Boudina†, E. Dale Abel†, Donald A. McClain†, and Jared Rutter\*\*

\*Department of Biochemistry and †Division of Endocrinology, Diabetes and Metabolism, University of Utah School of Medicine, Salt Lake City, UT 84112

Edited by Steven L. McKnight, University of Texas Southwestern Medical Center, Dallas, TX, and approved August 8, 2007 (received for review June 11, 2007)

The metabolic syndrome, a complex set of phenotypes typically associated with obesity and diabetes, is an increasing threat to global public health. Fundamentally, the metabolic syndrome is caused by a failure to properly sense and respond to cellular metabolic cues. We studied the role of the cellular metabolic sensor PAS kinase (PASK) in the pathogenesis of metabolic disease by using *PASK*<sup>-/-</sup> mice. We identified tissue-specific metabolic phenotypes caused by *PASK* deletion consistent with its role as a metabolic sensor. Specifically, *PASK*<sup>-/-</sup> mice exhibited impaired glucose-stimulated insulin secretion in pancreatic  $\beta$ -cells, altered triglyceride storage in liver, and increased metabolic rate in skeletal muscle. Further, *PASK* deletion caused nearly complete protection from the deleterious effects of a high-fat diet including obesity and insulin resistance. We also demonstrate that these cellular effects, increased rate of oxidative metabolism and ATP production, occur in cultured cells. We therefore hypothesize that PASK acts in a cell-autonomous manner to maintain cellular energy homeostasis and is a potential therapeutic target for metabolic disease.

metabolism | PAS domain | nutrient sensing | obesity

Because of changes in diet and lifestyle, the incidence of obesity and type 2 diabetes is increasing dramatically worldwide. Type 2 diabetes arises when pancreatic  $\beta$ -cells fail to secrete sufficient insulin to compensate for peripheral insulin resistance, a condition severely aggravated by obesity (1, 2). Type 2 diabetes is now widely viewed as a manifestation of a broader underlying metabolic disorder called the metabolic syndrome, which is characterized by hyperglycemia, hyperinsulinemia, dyslipidemia, hypertension, visceral obesity, and cardiovascular disease (3). The World Health Organization estimates that the current decade will witness a 46% increase in diabetes incidence worldwide (from 151 million to 221 million), with the vast majority of this increase being due to metabolic syndrome-related type 2 diabetes (4).

Cellular energy and nutrient sensors determine how cells respond to excessive nutrients, and aberrant nutrient and energy sensing is a contributing factor to metabolic syndrome development (5, 6). AMP-activated protein kinase (AMPK) and mammalian target of rapamycin (mTOR) are two well studied and evolutionarily conserved cellular energy and nutrient sensors. AMPK is activated in response to intracellular ATP depletion and acts to switch the cellular metabolic program from ATP consumption to ATP production (7). In contrast to AMPK, mTOR is activated by sufficient cellular energy or nutrients, particularly amino acids (8). Activation of mTOR stimulates cell growth by increasing protein synthesis through phosphorylation of ribosomal S6 kinase (S6K) and eIF4E-binding protein (9). Decreased AMPK activity and elevated mTOR activity have been linked with obesity, diabetes, and cancer (10–12).

Like AMPK and mTOR, PAS kinase (PASK) is a nutrient-responsive protein kinase conserved from yeast to humans. The PAS domain of PASK specifically interacts with the kinase catalytic domain and inactivates the kinase in cis (13). Based on biochemical and genetic data, a model has been proposed wherein a small

metabolite activates PASK by directly interacting with the PAS domain and disrupting its interaction with the kinase domain (5, 14, 15). Studies in cultured pancreatic  $\beta$ -cells support a role for PASK in nutrient sensing and response. Specifically, PASK has been shown to be regulated by glucose both posttranslationally and at the level of gene expression, and PASK activity is required for glucose-stimulated insulin expression in Min-6 cells (16).

We sought to address the *in vivo* role of PASK in pancreatic  $\beta$ -cell function and energy homeostasis. Using *PASK*<sup>-/-</sup> mice (17), we demonstrate that PASK is required for normal  $\beta$ -cell insulin secretion. We also demonstrate that *PASK* deletion results in resistance to the phenotypes caused by a high-fat diet, including obesity, insulin resistance, and hepatic triglyceride accumulation. This protection is likely due to increased metabolic rate and energy expenditure in *PASK*<sup>-/-</sup> mice independent of the activity of AMPK, mTOR, and peroxisome proliferator-activated receptor  $\gamma$  coactivator 1 (PGC-1). Increased oxidative metabolism and ATP generation are also observed in cultured cells upon acute PASK knockdown by RNAi. These cellular effects, which recapitulate effects observed *in vivo*, support the hypothesis that PASK functions as a cell-autonomous regulator of cellular energy balance (14).

## Results

**Impaired Glucose-Stimulated Insulin Secretion (GSIS) in *PASK*<sup>-/-</sup> Mice.** Previously, PASK was shown to be required for the induction of preproinsulin promoter activity by high glucose concentrations in cultured Min-6  $\beta$ -cells (16). To examine GSIS in *PASK*<sup>-/-</sup> mice, we measured plasma insulin levels before and after an intraperitoneal glucose injection. As shown in Fig. 1A, insulin levels in *PASK*<sup>-/-</sup> mice are modestly but significantly lower than those in WT littermates at both 5 min and 45 min after glucose injection. This defect in insulin secretion is also manifest in isolated islets of Langerhans *in vitro*. Using islet perfusion experiments, we found *PASK*<sup>-/-</sup> islets to be defective in GSIS, particularly at higher glucose concentrations (Fig. 1B), but normal in depolarization-induced insulin secretion (data not shown). The total insulin secreted by *PASK*<sup>-/-</sup> islets in these experiments was 56% the total secreted by WT islets.

Defects in insulin secretion are often accompanied by alterations in islet morphology or  $\beta$ -cell mass. To determine whether these

Author contributions: E.D.A., D.A.M., and J.R. designed research; H.-X.H., C.M.C., W.S., R.C.C., T.L.S., J.W., and S.B. performed research; H.-X.H., W.S., R.C.C., S.B., E.D.A., D.A.M., and J.R. analyzed data; and H.-X.H. and J.R. wrote the paper.

Conflict of interest statement: J.R. is a consultant to BioEnergenix, LLC.

This article is a PNAS Direct Submission.

Abbreviations: AMPK, AMP-activated protein kinase; mTOR, mammalian target of rapamycin; PASK, PAS kinase; PGC-1, peroxisome proliferator-activated receptor  $\gamma$  coactivator 1; GSIS, glucose-stimulated insulin secretion; GTT, glucose tolerance test; ITT, insulin tolerance test; HFD, high-fat diet; NCD, normal chow diet; PPAR $\gamma$ , peroxisome proliferator-activated receptor  $\gamma$ ; SCD1, stearoyl-CoA desaturase 1; PXR, pregnane X receptor; shRNA, short hairpin RNA.

\*To whom correspondence should be addressed. E-mail: rutter@biochem.utah.edu.

This article contains supporting information online at [www.pnas.org/cgi/content/full/0705407104/DC1](http://www.pnas.org/cgi/content/full/0705407104/DC1).

© 2007 by The National Academy of Sciences of the USA

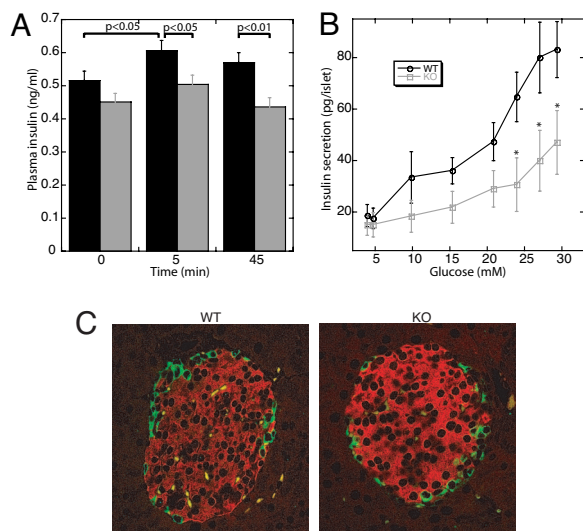


**Fig. 1.** Impaired insulin secretion but normal islet morphology in  $PASK^{-/-}$  mice. (A) Plasma insulin concentrations before and after i.p. glucose injection into WT (black bars) and  $PASK^{-/-}$  (gray bars) ( $n = 24$  male mice per genotype, 12 weeks of age). (B) Perfusion of 15–17 isolated islets with a 3–30 mM glucose ramp in gassed Krebs buffer for 40 min ( $n = 4$  female mice, 16 weeks of age). Area under the curve:  $1,146 \pm 129$  for WT islets and  $646 \pm 171$  for  $PASK^{-/-}$  islets ( $P < 0.05$ ). The experiment was performed twice with similar results. \*,  $P < 0.05$ . Data shown represent the mean  $\pm$  SD. (C) Immunostaining of pancreatic sections by using anti-insulin (red) and anti-glucagon (green) antibodies from 16-week-old male WT and  $PASK^{-/-}$  mice.

parameters are affected in  $PASK^{-/-}$  mice, we examined islet organization and morphology by glucagon and insulin double immunostaining. No defect in islet morphology, size, or  $\beta$ -cell area was observed in  $PASK^{-/-}$  mice (Fig. 1C and data not shown). We also observed no significant difference between WT and  $PASK^{-/-}$  mice in *Ins-1* or *Ins-2* mRNA levels (see supporting information (SI) Fig. 6A) or in total pancreatic insulin (SI Fig. 6B). The expression levels of several genes involved in insulin transcription and GSIS, including *Pdx-1*, *MafA*, *GLUT2*, and glucokinase, were also unchanged in  $PASK^{-/-}$  islets (data not shown). We therefore suggest that the GSIS defect observed in  $PASK^{-/-}$  mice is likely a result of impaired  $\beta$ -cell glucose sensing.

**Improved Glucose Tolerance, Increased Insulin Sensitivity, and Resistance to Obesity in High-Fat Diet (HFD)-Fed  $PASK^{-/-}$  Mice.** To assess whether PASK is required for the maintenance of glucose homeostasis, we performed a glucose tolerance test (GTT), in which plasma glucose levels were monitored over time after glucose injection.  $PASK^{-/-}$  mice displayed a slight and statistically insignificant glucose intolerance (Fig. 2A). Insulin sensitivity, as measured by insulin tolerance test (ITT), was identical in WT and  $PASK^{-/-}$  mice (Fig. 2B). When fed a HFD, C57BL/6J mice develop obesity and a set of symptoms reminiscent of the metabolic syndrome, including insulin resistance (18). To examine glucose homeostasis under this stress condition, we performed GTT and ITT experiments on HFD-fed WT and  $PASK^{-/-}$  mice. Whereas HFD-fed WT mice developed glucose intolerance and insulin resistance,  $PASK^{-/-}$  mice were completely protected from these effects (Fig. 2C and D; compare with Fig. 2A and B). As expected, fasting insulin levels of HFD-fed  $PASK^{-/-}$  mice were substantially lower than the fasting insulin levels of WT mice (SI Fig. 7A).

$PASK^{-/-}$  mice were also protected from HFD-induced obesity. WT and  $PASK^{-/-}$  mice were of similar weight on normal chow diet (NCD) (Fig. 2E), but the weight gain of  $PASK^{-/-}$  mice on HFD was significantly less than that of WT littermates (Fig. 2F). After 8 weeks of HFD feeding, the body weight of  $PASK^{-/-}$  mice was

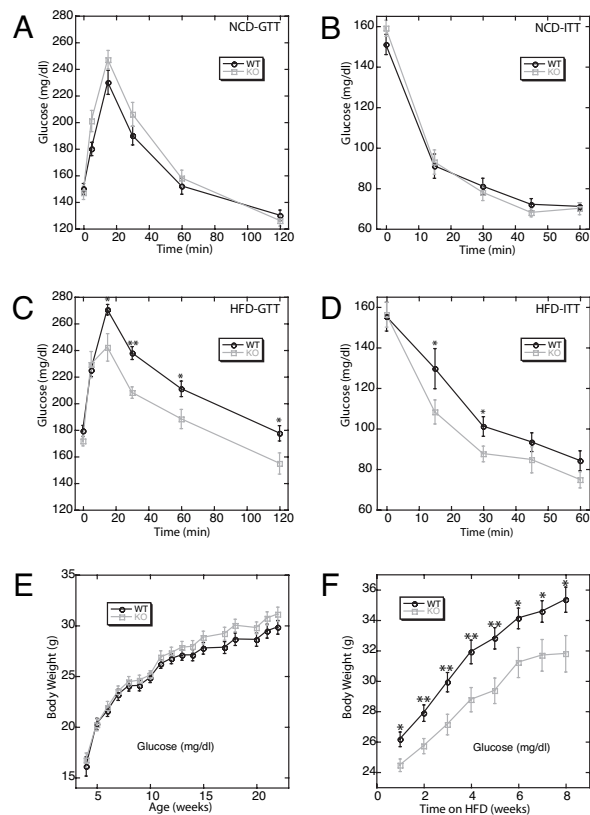


**Fig. 2.**  $PASK^{-/-}$  mice were protected from diet-induced glucose intolerance, insulin resistance, and obesity. (A–D) GTT and ITT with WT and  $PASK^{-/-}$  mice fed with either NCD (A and B) or HFD (C and D). Plasma glucose levels were determined before and at indicated times after i.p. glucose (A and C) or insulin (B and D) injection. (E and F) Growth curves of WT and  $PASK^{-/-}$  mice on NCD (E) or HFD (F) beginning at 12 weeks of age. All data represent the mean  $\pm$  SEM for 12 male mice of each genotype. \*,  $P < 0.05$ ; \*\*,  $P < 0.01$ .

similar to NCD-fed WT or  $PASK^{-/-}$  mice. Analysis of body composition by dual-energy x-ray absorptiometry showed that the difference in total body weight between WT and  $PASK^{-/-}$  HFD-fed mice is completely accounted for by decreased fat mass in  $PASK^{-/-}$  mice (SI Fig. 7B).

**$PASK^{-/-}$  Mice Exhibit Increased Whole-Body Energy Expenditure and Increased Metabolic Rate in Skeletal Muscle.** We hypothesized that the  $PASK^{-/-}$  lean phenotype is responsible for the improved glucose tolerance and insulin sensitivity; therefore, we sought to understand the basis for this phenotype. Obesity is the result of an imbalance between energy intake (in the form of feeding) and energy expenditure (in the form of physical activity and basal metabolism) (19). We therefore measured  $O_2$  consumption,  $CO_2$  production, food intake, and locomotor activity by using metabolic chambers. Food intake and locomotor activity were similar, but  $PASK^{-/-}$  mice consumed more  $O_2$ , produced more  $CO_2$ , and generated more heat than WT littermates (Fig. 3A). Relative to WT mice, HFD-fed  $PASK^{-/-}$  mice have a slight substrate preference for carbohydrate over fat, as indicated by the respiratory quotient ( $0.91 \pm 0.02$  for WT mice and  $0.93 \pm 0.02$  for  $PASK^{-/-}$  mice,  $P < 0.05$ , night values). This hypermetabolic phenotype in  $PASK^{-/-}$  mice was also manifest in permeabilized soleus muscle fibers, wherein we observed elevated ATP production from succinate in  $PASK^{-/-}$  muscle (Fig. 3B).

One potential explanation for the observed increase in oxidative metabolism was an increase in mitochondrial mass in  $PASK^{-/-}$  muscle. However, soleus muscle electron micrographs (Fig. 3C) and



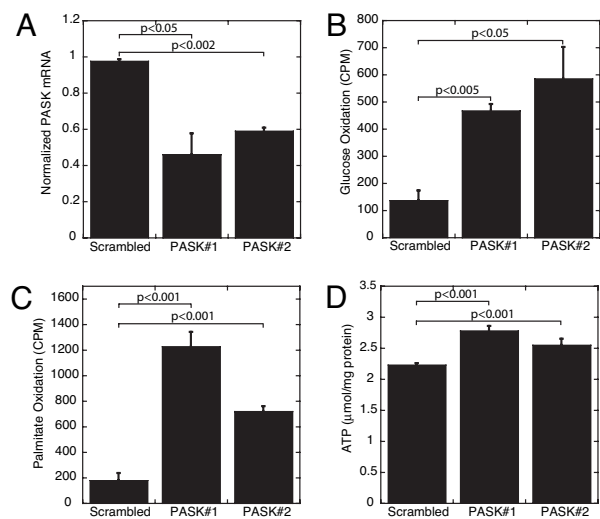


**Fig. 5.** Increased oxidative metabolism and cellular ATP content upon PASK silencing in L6 cells. (A) PASK mRNA levels in L6 clones expressing either scrambled or PASK shRNA in the absence of doxycycline. Data represent the mean  $\pm$  SD of triplicates per group. (B) Measurement of  $^{14}\text{C}$  released from indicated L6 clones incubated in [ $^{14}\text{C}$ ]glucose ( $n = 3$ ). (C) Measurement of  $^{14}\text{C}$  released from indicated L6 clones incubated in [ $^{14}\text{C}$ ]palmitate ( $n = 3$ ). (D) Cellular ATP content measurement normalized to protein in extract.

We also determined the levels of transcripts related to lipid metabolism in liver from HFD-fed WT and *PASK*<sup>-/-</sup> mice. Levels of stearoyl-CoA desaturase 1 (SCD1) (27), long-chain fatty acid elongase (28), fatty acid transporter (CD36) (29), and the lipid-responsive nuclear hormone receptor peroxisome proliferator-activated receptor  $\gamma$  (PPAR $\gamma$ ) (30) are all significantly decreased in *PASK*<sup>-/-</sup> liver (Fig. 4D). Lower expression of each of these genes is consistent with decreased hepatic lipid synthesis and triglyceride accumulation. The transcripts of other genes involved in fatty acid metabolism, including *FAS*, *ACC-1*, and *SREBP-1c*, showed no difference between WT and *PASK*<sup>-/-</sup> liver (Table 1).

The altered lipid accumulation and the pattern of gene expression observed in *PASK*<sup>-/-</sup> liver is strikingly similar, albeit opposite, to that observed in a transgenic mouse expressing a constitutively active pregnane X receptor (PXR) in liver (31). This observation raised the possibility that the PASK-dependent effects on lipid metabolism in liver might be mediated through a decrease in PXR expression or function. Indeed, we observed a decrease in the mRNA levels of a well established PXR target gene *CYP3A11* (32) in *PASK*<sup>-/-</sup> liver. The expression of the *PXR* gene itself is not altered by *PASK* deletion (Fig. 4D); therefore, if PASK does regulate PXR activity, it does so via a mechanism distinct from gene expression.

#### Acute PASK Silencing Increases Oxidative Metabolism in Cultured Cells.

To address the possibility that the observed hypermetabolic phenotype in skeletal muscle is a secondary or adaptive response to *PASK* deletion in mice, we generated two independent L6 myoblast cell lines wherein we could acutely silence PASK expression by using short hairpin RNA (shRNA) upon doxycycline removal. As shown in Fig. 5A, these two clones both exhibit an  $\approx 50\%$  decrease in PASK mRNA upon doxycycline removal compared with the scrambled shRNA control. On PASK knockdown, we observed a large increase in both glucose and palmitate oxidation (Fig. 5B and C). This increased substrate metabolism is accompanied by elevated steady-state levels of ATP, presumably a result of increased mitochondrial ATP production (Fig. 5D). We also generated L6-derived cells with constitutive knockdown of PASK and observed increased glucose oxidation and ATP levels (data not

shown). These data in cultured cells indicate that loss of PASK leads to an acute and cell-autonomous increase in mitochondrial metabolism and ATP production.

#### Discussion

Herein we describe a physiological role for PASK in regulating mammalian energy balance. *PASK*<sup>-/-</sup> mice are protected from HFD-induced obesity and from other metabolic perturbations that accompany HFD-induced obesity. Levels of insulin sensitivity and glucose tolerance in HFD-fed *PASK*<sup>-/-</sup> mice are nearly identical to the levels in NCD-fed WT or *PASK*<sup>-/-</sup> mice. These changes in organismal energy and glucose homeostasis are likely manifestations of an underlying alteration in metabolic regulation in individual cells and tissues. We have previously described a role for PASK in glucose-responsive processes in pancreatic  $\beta$ -cells (16). We show here that *PASK*<sup>-/-</sup> mice exhibit hypoinsulinemia *in vivo* and *PASK*<sup>-/-</sup> islets have impaired GSIS *in vitro*. These effects are not due to decreased insulin gene expression or altered islet morphology or mass, but likely to impaired  $\beta$ -cell glucose sensing. Another group did not observe this decrease in GSIS in *PASK*<sup>-/-</sup> mice (33).

We observed a striking protection from HFD-induced hepatic steatosis in *PASK*<sup>-/-</sup> mice. This is accompanied by a significant decrease in the transcript levels of SCD1, fatty acid elongase, CD36, and PPAR $\gamma$ . SCD1 is the rate-limiting enzyme in the synthesis of monounsaturated fatty acids, which are the major substrates for triglyceride synthesis (34). *SCD1*<sup>-/-</sup> mutant mice exhibit decreased liver triglyceride accumulation and fatty acid biosynthesis and are protected from HFD-induced obesity (35, 36). Fatty acid elongase is required for *de novo* fatty acid synthesis (37). CD36 (also known as fatty acid translocase) is a putative fatty acid transporter. Interestingly, *CD36* is a target gene of PPAR $\gamma$  (38); thus, the decreased expression of *CD36* could be secondary to the lower expression of PPAR $\gamma$  in *PASK*<sup>-/-</sup> liver. PPAR $\gamma$  expression has been shown to positively correlate with obesity in multiple mouse models (39). Decreased expression of each of these genes in liver is consistent with decreased lipid content observed in HFD-fed *PASK*<sup>-/-</sup> mice. These alterations in gene expression, and particularly a decrease in *CYP3A11* expression, are consistent with decreased PXR activity in *PASK*<sup>-/-</sup> liver (31). The expression of *PXR* is not different, however, suggesting that PASK might regulate PXR via direct phosphorylation, through altered abundance of a PXR agonist, or through other mechanisms. Alternatively, the PXR paralog CAR, which activates an overlapping set of genes, might be down-regulated upon *PASK* deletion. These hypotheses await further investigation.

Deletion of *PASK* leads to organismal hypermetabolism as measured by  $\text{O}_2$  consumption,  $\text{CO}_2$  production, and heat generation. This hypermetabolism is also exhibited in isolated permeabilized skeletal muscle, wherein we observed increased ATP production. A number of mouse models exhibit similar hypermetabolism. Three aspects of the *PASK*<sup>-/-</sup> phenotype make it unusual. First, the elevated metabolic rate is not caused by impaired metabolic efficiency and concomitantly increased substrate demand. In fact, we observed increased ATP production both in isolated *PASK*<sup>-/-</sup> skeletal muscle and in cultured cells upon acute *PASK* knockdown. Further, energy stress is not apparent, as there is no AMPK hyperactivation in liver or skeletal muscle from *PASK*<sup>-/-</sup> mice as measured by phosphorylation of either AMPK or ACC (Fig. 4C and data not shown). Second, the increased mitochondrial oxidative metabolism occurs without changes in mitochondrial mass or number or in PGC-1 $\alpha$  or - $\beta$  expression. Third, this phenotype seems to be a property of individual cells because it is recapitulated in L6 myoblasts upon acute *PASK* knockdown. Although the detailed mechanism for increased oxidative metabolism upon *PASK* loss is unclear, it is almost certainly due to changes in mitochondria. First, the *ex vivo* soleus ATP measurements were performed under conditions that measure mitochondrial ATP production. Second,

the observation that both glucose and palmitate oxidation were increased upon PASK knockdown suggests that the alteration lies downstream of where these two metabolic pathways converge, namely at the level of the mitochondrial tricarboxylic acid cycle.

We have previously proposed that PASK functions as a cell-autonomous nutrient sensor (5, 14). PASK is posttranslationally activated by elevated glucose medium in cultured  $\beta$ -cells (16), probably through allosteric control via its regulatory PAS domain (13, 15). PASK also is regulated by nutrient status at the level of gene expression (16). Taking these observations together, we conclude that PASK integrates multiple cues to monitor cellular energetic status. As inferred from the loss-of-function phenotype, the effect of PASK activation seems to be cell type specific and part of an appropriate nutrient response for each cell type analyzed. PASK activation in  $\beta$ -cells contributes to insulin secretion. PASK activation in hepatocytes increases the synthesis and accumulation of storage lipids such as triglycerides. PASK activation in skeletal muscle results in decreased ATP generation both from carbohydrate and fatty acid oxidation. We, therefore, propose a model wherein PASK acts as a sensor, integrator, and transducer of a metabolic sufficiency signal. The transduction pathway downstream of PASK is cell type specific but, at least in skeletal muscle, decreases mitochondrial oxidative metabolism and ATP production. When PASK is artificially lost, this metabolic sufficiency signal is not transduced and the result is chronically elevated mitochondrial metabolism, resulting in protection from ectopic HFD-induced lipid accumulation. As with the other well known metabolic sensory kinases AMPK and mTOR, we propose that PASK may be an important regulator of human metabolic disease.

## Methods

**Animals.** *PASK*<sup>-/-</sup> mice were genotyped as described (17). After the fifth backcross into C57BL/6 (Charles River Laboratories, Wilmington, MA), 12- to 24-week-old males were used for all experiments except that the islet perfusion studies were performed on females. Mice were maintained on a NCD (3080; Harlan Teklad, Madison, WI) or a HFD from 12 weeks of age (45% fat by calories, D12451; Research Diets, New Brunswick, NJ). In each experiment, age-matched WT littermates were used as controls for *PASK*<sup>-/-</sup> mice. All procedures were approved by the institutional animal care and use committee of University of Utah.

**Cell Culture.** Rat L6 myoblasts were provided by Scott Summers (University of Utah, Salt Lake City, UT). Cells were maintained at 37°C under 5% CO<sub>2</sub> in DMEM supplemented with 10% FBS (HyClone, Logan, UT), 0.1 mg/ml penicillin and 0.1 mg/ml streptomycin (Life Technologies, Grand Island, NY).

**GTT/ITT and Serum Insulin Measurement.** For GTT and plasma insulin measurement, experimental animals were fasted for 6 h, after which glucose (1 g/kg body weight) was injected i.p. At the indicated times, tail vein blood was sampled for glucose determination with a glucometer (Bayer, Pittsburgh, PA) or for insulin measurement by using the Sensitive Rat Insulin RIA kit (Linco Research, St. Charles, MO). For ITT, human recombinant insulin (0.75 unit/kg of body weight; Novo-Nordisk, Copenhagen, Denmark) was injected i.p. to randomly fed mice and blood glucose levels were determined at the indicated times.

**Islet Isolation and Perfusion.** Islets of Langerhans were isolated from pancreas by using the intraductal liberase (Roche Applied Science, Indianapolis, IN) digestion method as described in ref. 40. Fifteen to 17 size-matched islets were individually handpicked and used for perfusion experiments as described (40). The glucose and released insulin in fractions of perfusion buffer were measured by using a Glucose Analyzer (Beckman Instruments, Fullerton, CA) and Sensitive Rat Insulin RIA kit (Linco Research), respectively.

**Metabolic Chamber Studies.** Indirect calorimetry was performed with a four-chamber Oxymax system (Columbus Instruments, Columbus, OH). Animals were allowed to adapt to the metabolic chamber for 4 h and then VO<sub>2</sub>, VCO<sub>2</sub>, heat production, food and water intake, and movement were measured every 15 min for 3 days from individually housed mice. Averaged data from 6 p.m. to 6 a.m. are expressed as night values and data from 6 a.m. to 6 p.m. are expressed as day values.

**Mitochondrial Respiration Experiment.** Soleus fibers were separated and then permeabilized by saponin. Maximal (ADP-stimulated) ATP production rate was determined by exposing fibers to 1 mM exogenous ADP and succinate as described (21).

**Citrate Synthase Activity Assay.** Citrate synthase activity was measured by the spectrophotometric method as described (41). In brief, frozen soleus muscle was homogenized on ice and citrate synthase was released from mitochondria by freezing and thawing the homogenate. The reaction was initiated by addition of oxaloacetate into 1 ml of diluted homogenate in reaction buffer containing acetyl-CoA, and then monitored at 412 nm for 3 min with an Ultrospec 3000 spectrophotometer (Amersham, Piscataway, NJ).

**Histological Analysis.** For immunostaining, dissected pancreata were fixed overnight at room temperature in 10% formalin, paraffin-embedded, and microtome-sectioned at 5  $\mu$ m thickness. After deparaffinization and rehydration, the sections were sequentially treated with 3% H<sub>2</sub>O<sub>2</sub>, target retrieval solution (DAKO, Glostrup, Denmark), and blocking solution. The sections were then incubated with antiglucacon (Vector Laboratories, Burlingame, CA), followed by secondary antibody labeled with AlexaFluor 488 (Molecular Probes, Carlsbad, CA), and anti-insulin (DAKO), followed by AlexaFluor 594-labeled secondary antibody. Fluorescent confocal images were captured, overlaid, and analyzed by National Institutes of Health (NIH) ImageJ software. For electron microscopy analysis, soleus muscle was fixed in EM fixative, dehydrated in graded ethanol, and embedded in Poly Bed plastic resins for sectioning as described (21). Soleus mitochondrial number was quantified in blinded fashion from electron micrographs at the magnification of  $\times$ 8000 and normalized to Z line number. For oil red O staining, frozen liver samples were embedded in OTC reagent (Tissue-Tek; Sakura Finetek, Hatfield, PA) and sectioned at 8  $\mu$ m in cryostat. Cryosections were fixed in formaldehyde vapor at 50°C, incubated in 0.5% oil red O in isopropyl alcohol, and counterstained with hematoxylin (Sigma, St. Louis, MO). After rinsing in distilled water, liver sections were mounted with permanent aqueous mounting medium Gel/Mount (Biomed, Foster City, CA) and photographed by using light microscopy at  $\times$ 40 magnification. All images were acquired at the University of Utah Imaging Core Facility.

**Liver Triglyceride Content Measurement.** Quantitative analysis of liver triglyceride content was performed by saponification of liver in ethanolic KOH as described (42). After neutralization with MgCl<sub>2</sub>, glycerol produced during hydrolysis was measured by a colorimetric assay with Free Glycerol Reagent and Glycerol Standard Solution (Sigma).

**Western Blotting.** Liver lysates were prepared by homogenizing 50–100 mg snap-frozen liver slices in cell lysis buffer (Cell Signaling Technology, Beverly, MA) by using a Tissue-Tearer rotor. After centrifugation at 20,000  $\times$  g for 30 min at 4°C, the supernatants were collected and protein concentrations were determined by Advanced Protein Assay Reagent (Cytoskeleton, Denver, CO). About 50  $\mu$ g of protein from each sample was separated by SDS/PAGE, transferred to a PVDF membrane (Fisher, Waltham, MA), and blotted with indicated antibodies according to the manufacturer's

protocol. Phospho-AMPK (Thr-172), phospho-S6K (Thr-389), and tubulin antibodies were purchased from Cell Signaling Technology.

**Real-Time Quantitative RT-PCR.** Total RNA was extracted from tissues or cells by using RNeasyStat60 reagent (Tel-Test, Friendswood, TX) and purified with RNeasy Mini kit (Qiagen, Valencia, CA), according to the manufacturer's instructions. First-strand cDNA synthesis was carried out with SuperScript III reverse transcriptase (Invitrogen, Carlsbad, CA). Real-time PCR was performed on a LightCycler (Roche Diagnostics, Indianapolis, IN) by using the SYBR Green-based method as described (40). Melting curve analysis and a mock reverse transcribed control were included to ensure the specificity of the amplicons. Primer sequences for indicated transcripts are available on request.

**Generation of Inducible PASK Knockdown Cells.** pRevTet-Off-IN retroviral vector was purchased from Clontech (Mountain View, CA), and retrovirus was produced according to the manufacturer's instructions by using Fugene transfection reagent (Roche Applied Science) and Phoenix-Ampho retroviral packaging cell line (American Type Culture Collection, Manassas, VA). L6 cells were infected with the generated Tet-Off retrovirus in the presence of 6 mg/ml Polybrene, and 48 h after infection G418 was added to the medium at a final concentration of 200  $\mu$ g/ml. After 2 weeks of selection, G418-resistant colonies were individually harvested by using cloning cylinders (Corning, Corning, NY) and screened for inducibility with pRevTRE-Luc (Clontech) virus. shRNA oligonucleotide duplexes containing sequences targeting rat PASK gene and a scrambled shRNA were designed by using Invitrogen web site software and cloned into tetracycline-regulated retroviral SIN-TREmiR30-PIG (TMP) vector (OPEN Biosystems, Huntsville, AL). Retrovirus expressing the inducible hairpins was generated and used to infect highly inducible Tet-Off L6 clones as verified by luciferase assay. Finally, 2  $\mu$ g/ml puromycin as well as 2  $\mu$ g/ml doxycycline was applied and puromycin-resistant clones were isolated as described above. PASK knockdown clones were screened by quantitative RT-PCR analysis of PASK mRNA levels in the absence and presence of doxycycline. PASK targeting hairpin sequence: GATGCCAAGACCACAGAGA and GCGCAGACAAGCTCAAAGA. Scrambled sequence: GCGCAGACAAGCTCAAAGA.

**Glucose and Palmitate Oxidation Measurement.** Glucose oxidation rates were determined according to previously described methods (43). In brief, triplicate samples of L6 cells were incubated with 500  $\mu$ l of oxygenated Krebs-Ringer buffer containing 5 mM unlabeled glucose, 2  $\mu$ Ci of [U- $^{14}$ C]glucose (MP Biochemicals, Aurora, OH), and 0.4% BSA (wt/vol) in a 24-well plate. A UniFilter-24 GF/B plate (Packard Instruments, Waltham, MA) was sealed with an adhesive sheet by using vacuum grease, and 200  $\mu$ l of 10 $\times$  hyamine hydroxide (PerkinElmer Sciences, Waltham, MA) was pipetted onto each filter for CO<sub>2</sub> capture. Finally, the 24-well plate was sealed with a rubber gasket. The apparatus was incubated with gentle shaking for 2 h at 37°C and the experiment was stopped by injecting 100  $\mu$ l of 1 M perchloric acid per well. Filters were removed, and captured  $^{14}$ CO<sub>2</sub> was measured by scintillation counting. Control incubations lacking cells were included in each plate. For palmitate oxidation, the same procedure was used except using Krebs-Ringer buffer containing 1 mM glucose, 0.5 mM unlabeled palmitate, 1  $\mu$ Ci of [1- $^{14}$ C]palmitate (MP Biochemicals), and 1 mM carnitine.

**Cellular ATP Content Measurement.** L6 cells were washed with PBS, harvested by trypsinization, and pelleted by centrifugation. The cells were then lysed in 1 M perchloric acid on ice to precipitate cellular proteins. After centrifugation at 20,000  $\times$  g for 10 min, the supernatant was transferred into a new tube and neutralized with an equal volume of 1 M KOH. The ATP content was measured by an ATP Determination kit (Invitrogen) according to the manufacturer's instructions.

**Statistical Analysis.** Data are presented as mean  $\pm$  standard deviation unless otherwise indicated. A two-tailed equal variance *t* test was used to compare differences, and the null hypothesis was rejected at the 0.05 level.

We thank Scott Summers for the parental L6 cell line and for helpful discussions, Dean Tantin for the Phoenix-Ampho cell line, Janet Lindley for helpful discussions, and Roland H. Wenger for the PASK<sup>-/-</sup> mice. This work was supported by National Institutes of Health Grant DK071962 (to J.R.), an American Diabetes Association Career Development Award (to J.R.), and a Searle Scholars Award (to J.R.).

- Rhodes CJ (2005) *Science* 307:380–384.
- Lazar MA (2005) *Science* 307:373–375.
- Reaven GM (1988) *Diabetes* 37:1595–1607.
- Zimmet P, Alberti KG, Shaw J (2001) *Nature* 414:782–787.
- Lindsay JE, Rutter J (2004) *Comp Biochem Physiol B Biochem Mol Biol* 139:543–559.
- Marshall S (2006) *Sci STKE* 2006:re7.
- Hardie DG, Carling D, Carlson M (1998) *Annu Rev Biochem* 67:821–855.
- Proud CG (2002) *Eur J Biochem* 269:5338–5349.
- Gingras AC, Raught B, Sonenberg N (2001) *Genes Dev* 15:807–826.
- Inoki K, Corradetti MN, Guan KL (2005) *Nat Genet* 37:19–24.
- Winder WW, Hardie DG (1999) *Am J Physiol* 277:E1–E10.
- Manning BD (2004) *J Cell Biol* 167:399–403.
- Rutter J, Michnoff CH, Harper SM, Gardner KH, McKnight SL (2001) *Proc Natl Acad Sci USA* 98:8991–8996.
- Rutter J (2002) *Science* 298:1567–1568.
- Amezua CA, Harper SM, Rutter J, Gardner KH (2002) *Structure (London)* 10:1349–1361.
- da Silva Xavier G, Rutter J, Rutter GA (2004) *Proc Natl Acad Sci USA* 101:8319–8324.
- Katschinski DM, Marti HH, Wagner KF, Shibata J, Eckhardt K, Martin F, Depping R, Paasch U, Gassmann M, Ledermann C, et al. (2003) *Mol Cell Biol* 23:6780–6789.
- Surwit RS, Kuhn CM, Cochrane R, McCubbin JA, Feinglos MN (1988) *Diabetes* 37:1163–1167.
- Spiegelman BM, Flier JS (2001) *Cell* 104:531–543.
- Leek BT, Mudaliar SR, Henry R, Mathieu-Costello O, Richardson RS (2001) *Am J Physiol* 280:R441–R447.
- Leone TC, Lehman JJ, Finck BN, Schaeffer PJ, Wende AR, Boudina S, Courtois M, Wozniak DF, Sambandan M, Bernal-Mizrachi C, et al. (2005) *PLoS Biol* 3:e101.
- Puigserver P, Wu Z, Park CW, Graves R, Wright M, Spiegelman BM (1998) *Cell* 92:829–839.
- Unger RH (2002) *Annu Rev Med* 53:319–336.
- Voshol PJ, Haemmerle G, Ouwens DM, Zimmermann R, Zechner R, Teusink B, Maassen JA, Havekes LM, Romijn JA (2003) *Endocrinology* 144:3456–3462.
- Um SH, Frigerio F, Watanabe M, Picard F, Joaquin M, Sticker M, Fumagalli S, Allegrini PR, Kozma SC, Auwerx J, Thomas, G (2004) *Nature* 431:200–205.
- Zhou G, Myers R, Li Y, Chen Y, Shen X, Fenyk-Melody J, Wu M, Ventre J, Doebber T, Fujii N, et al. (2001) *J Clin Invest* 108:1167–1174.
- Flowers MT, Miyazaki M, Liu X, Ntambi JM (2006) *J Clin Invest* 116:1478–1481.
- Matsuzaka T, Shimano H, Yahagi N, Yoshikawa T, Amemiya-Kudo M, Hasty AH, Okazaki H, Tamura Y, Iizuka Y, Ohashi K, et al. (2002) *J Lipid Res* 43:911–920.
- Schaffer JE (2002) *Am J Physiol* 282:E239–E246.
- Matsusue K, Haluzik M, Lambert G, Yim SH, Gavrilova O, Ward JM, Brewer B, Jr, Reitman ML, Gonzalez FJ (2003) *J Clin Invest* 111:737–747.
- Zhou J, Zhai Y, Mu Y, Gong H, Uppal H, Toma D, Ren S, Evans RM, Xie W (2006) *J Biol Chem* 281:15013–15020.
- Goodwin B, Redinbo MR, Klierer SA (2002) *Annu Rev Pharmacol Toxicol* 42:1–23.
- Bortner E, Niessen M, Zuellig R, Spinass GA, Spielmann P, Camenisch G, Wenger RH (2007) *Diabetes* 56:113–117.
- Dobrzyn A, Ntambi JM (2005) *Obes Rev* 6:169–174.
- Miyazaki M, Kim YC, Gray-Keller MP, Attie AD, Ntambi JM (2000) *J Biol Chem* 275:30132–30138.
- Ntambi JM, Miyazaki M, Stoehr JP, Lan H, Kendziorski CM, Yandell BS, Song Y, Cohen P, Friedman JM, Attie AD (2002) *Proc Natl Acad Sci USA* 99:11482–11486.
- Jakobsson A, Westerberg R, Jacobsson A (2006) *Prog Lipid Res* 45:237–249.
- Tontonoz P, Nagy L, Alvarez JG, Thomazy VA, Evans RM (1998) *Cell* 93:241–252.
- Memon RA, Tecott LH, Nonogaki K, Beigneux A, Moser AH, Grunfeld C, Feingold KR (2000) *Endocrinology* 141:4021–4031.
- Cooksey RC, Jouihan HA, Ajioka RS, Hazel MW, Jones DL, Kushner JP, McClain DA (2004) *Endocrinology* 145:5305–5312.
- Boudina S, Sena S, O'Neill BT, Tathireddy P, Young ME, Abel ED (2005) *Circulation* 112:2686–2695.
- Norris AW, Chen L, Fisher SJ, Szanto I, Ristow M, Jozsi AC, Hirshman MF, Rosen ED, Goodyear LJ, Gonzalez FJ, et al. (2003) *J Clin Invest* 112:608–618.
- Antinozzi PA, Segall L, Prentki M, McGarry JD, Newgard CB (1998) *J Biol Chem* 273:16146–16154.